Symposium - Original Research

Biomechanical model-based deformable registration of MRI and histopathology for clinical prostatectomy

Navid Samavati[1], Deirdre M. McGrath[2], Jenny Lee[2], Theodorus van der Kwast[3], Michael Jewett[4], Cynthia Ménard[2,5], Kristy K. Brock[1,2,5]

[1]Institute of Biomaterials and Biomedical Engineering, University of Toronto, [2]Radiation Medicine Program, Princess Margaret Hospital, [3]Department of Pathology, Toronto General Hospital, [4]Department of Surgery, Division of Urology, Princess Margaret Hospital, Toronto, [5]Department of Radiation Oncology, University of Toronto, Ontario, Canada

E-mail: *Kristy K. Brock - Kristy.Brock@rmp.uhn.on.ca
*Corresponding author

Abstract

A biomechanical model-based deformable image registration incorporating specimen-specific changes in material properties is optimized and evaluated for correlating histology of clinical prostatectomy specimens with *in vivo* MRI. In this methodology, a three-step registration based on biomechanics calculates the transformations between histology and fixed, fixed and fresh, and fresh and *in vivo* states. A heterogeneous linear elastic material model is constructed based on magnetic resonance elastography (MRE) results. The *ex vivo* tissue MRE data provide specimen-specific information for the fresh and fixed tissue to account for the changes due to fixation. The accuracy of the algorithm was quantified by calculating the target registration error (TRE) by identifying naturally occurring anatomical points within the prostate in each image. TRE were improved with the deformable registration algorithm compared to rigid registration alone. The qualitative assessment also showed a good alignment between histology and MRI after the proposed deformable registration.

Key words: Biomechanical models, correlative pathology, deformable registration, finite element model, magnetic resonance elastography

Access this article online

Website:
www.jpathinformatics.org

DOI: 10.4103/2153-3539.92035

Quick Response Code:

INTRODUCTION

Radiation therapy (RT) is a primary and effective modality to treat and often cure cancer.[1] To deliver this treatment, high resolution diagnostic-quality images (e.g., CT and MR) are necessary for the process of identifying and delineating the tumor and planning the radiation dose. Although, there have been remarkable developments in the imaging technology and dose delivery devices, many studies have shown that inaccuracies in the definition of the tumor boundaries have contributed to most of the post-treatment side effects.[2] The ability to compare and validate imaging with the gold standard of the histopathology is a key approach to overcoming this limitation.[3] Although this comparison is beneficial for advancement of RT, it is challenging due to the substantial changes that occur during the process of histology including gross tissue sectioning, processing, paraffin embedding, and fine sectioning to create histology slices. The main solution to compensate for the changes in the tissue is deformable registration.

Several different approaches to match histology slices with MRI have been investigated and reported in the literature. Solutions can be generally classified based on

the choice of nonrigid transformation employed in the algorithm.

One technique is to use free-form deformations (FFD) as the transformation, which was first proposed by Rueckert *et al.*[4] for the application of breast MRI. Dauguet *et al.*[5] used the "blockface" or the digital photographs of the sectioned baboon brain slices to assist in the registration of histology to MR. In their approach, blockface images were registered to MRI using mutual information-based FFD. They applied the resulting deformation field to the histology images, which were previously rigidly registered to the blockface images. Alic *et al.*[6] registered a dense histology volume, reconstructed by up to 100 histology slides of a xenograft tumor developed in a mouse, using a mutual information-based FFD to *in vivo* MRI via an intermediate *ex vivo* MRI. These two mentioned works[5,6] are based on intermediate registration and the registration performances were qualitatively shown to be good. However, no quantitative measures of registration accuracy is reported and the performance of their algorithm is highly dependent on the number of histology slices which is limited (around 10) for the case of prostatectomy.

Recently, Chappelow *et al.*[7] developed an algorithm based on multiattribute combined mutual information (MACMI) to benefit from all the information provided in multiprotocol MR. After finding the corresponding slices between histology and MRI of prostate, a 2D FFD registration by MACMI was applied to histology to match with MRI. Mazaheri *et al.*[8] used a similar approach for matching MRI and histology of prostate with a simpler optimization objective function to drive the 2D FFD registration. Their objective function was based on volume overlap of the prostate on MRI and histology. Both of these works[7,8] were based on corresponding 2D histology and MR image slices which limits the registration accuracy to be meaningful only in the plane of imaging.

The second group applies thin plate spline (TPS) to transform the images. An average TRE of 0.82 mm and 6% error in volume alignment was achieved by Zhan *et al.*[9] to match *ex vivo* MRI and histology in five prostate specimens. The registration was performed using 3D TPS based on boundary landmarks and automatically detected internal landmarks. Although the methodology of this work is promising for histology to *ex vivo* registration, automatic finding of corresponding landmarks between *in vivo* and histology is a difficult task that has not been investigated yet. Ward *et al.*[10] developed an image-based slicing method to accurately section the prostate specimens parallel to *in vivo* MR imaging plane. They achieved TRE of 0.85 mm by warping the 2D slices of MRI to their corresponding histology slides. However, their registration does not account for any out-of-plane deformation which can occur during gross sectioning and microtome slicing.

In a recent work by Ceritoglu *et al.*,[11] large deformation diffeomorphic metric mapping (LDDMM) was used to achieve an average surface distance of 0.4 mm between corresponding areas on histology images and MRI of nine monkey brains. The accuracy of the algorithm was improved by incorporating manually segmented regions of interest. LDDMM guarantees a one-to-one relationship between the registered images. Nonetheless, the applicability of this algorithm is highly influenced by the image intensity profile of the modalities used in registration. The intensity profiles can be affected by histology artifacts (tears, fissures, and missing tissue).

The last general approach is based on biomechanically derived transformations. McNiven *et al.*[12] used a biomechanical-based registration to match histology images of the prostate with *in vivo* MRI. Appropriate material property models derived from the literature were used in this initial investigation. The approach was based on rigidly reconstructed histology which resulted in average TRE distribution of 1.3, 1.2, and 1.9 mm in the left/right, anterior/posterior, and superior/inferior directions, respectively.

In this paper, an optimum biomechanical-based deformable registration is proposed to register whole-mount histology images to *in vivo* MRI of prostate. The mechanical behavior of the prostate 3D model is optimized by assigning specimen-specific material properties obtained using an *ex vivo* quasi-static magnetic resonance elastography (MRE) technique[13] for prostate specimens. A three-step deformable registration workflow is used to register histology images to *in vivo* MRI [Figure 1]. The histology slices are also reconstructed based on a 2D deformable registration technique. Compared to the relevant literature mentioned above, the proposed technique is minimally dependent on the number of histology slides and is fully performed in 3D and therefore it can account for out-of-plane deformations. It is primarily based on finding boundary alignment for driving the registration rather than image intensities which might fail due to artifacts and distortion on the images. Analysis of the registration accuracy is performed by calculating TRE to quantify the accuracy measurements and by visual inspection of the registered images. This work is a feasibility study and an initial proof of concept. Further experiments and comparisons with other well-known deformable registration algorithms are on going.

MATERIALS AND METHODS

Image Acquisitions
Seven sets of images are acquired for each of four patients
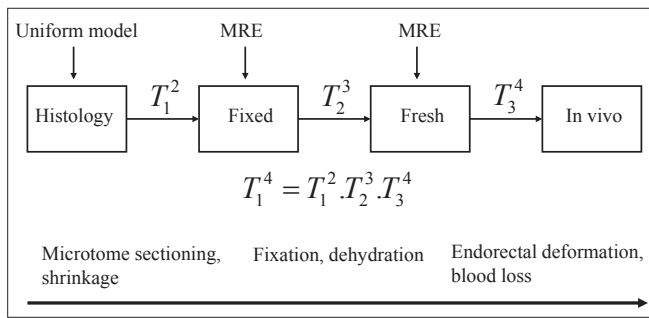
Figure 1: Summary of the deformable registration workflow. The process starts by registering histology to fixed, and then fixed to fresh, and finally fresh to *in vivo*. For the last two steps MRE-derived material properties are added to the biomechanical modeling

who have undergone radical prostatectomy:

1. *In vivo* T_2-weighted (T2w) MR images prior to prostatectomy, $0.27 \times 0.27 \times 3$ mm mm voxel size (termed "*in vivo*").
2. *Ex vivo* fresh T2w MR images of the prostate before fixation, $0.3 \times 0.3 \times 0.3$ mm voxel size ("fresh").
3. *Ex vivo* fresh MRE of the prostate before fixation, $0.5 \times 0.5 \times 3$ mm voxel size ("fresh MRE").
4. *Ex vivo* fixed T2w MR images of the prostate after fixation, $0.3 \times 0.3 \times 0.3$ mm voxel size ("fixed").
5. *Ex vivo* fixed MRE of the prostate after fixation, $0.5 \times 0.5 \times 3$ mm mm voxel size ("fixed MRE").
6. Digital gross photographs of the sectioned slices with 3 mm thickness ("gross").
7. Digital images of the whole-mount histology slides with 4 μm thickness ("histology").

The *in vivo* MR scans are obtained 3-5 weeks prior to surgery using an endorectal coil, where the imaging plane is set to be perpendicular to the endorectal coil. For whole-specimen fixation the prostatectomy specimens are submersed in 10% neutral-buffered formaldehyde solution for approximately 60 hours to insure complete penetration of fixative. Histology slides are carefully prepared by experienced pathology technicians to minimize damage to the tissue and distortion of the digitized histology images.

Tissue Sectioning Process
To obtain histology slides that are similar to *in vivo* images, the specimen must be cut at the same angles as the *in vivo* MR imaging planes. Therefore, the angle of cutting with respect to the resected specimen needs to be estimated. Based on the initial experiments, the most effective angle to best match the sectioned tissue slices with *in vivo* imaging plane is the rotation angle about left to right axis which is denoted by θ throughout this manuscript. Depending on the availability of gold seeds fiducial markers in the prostate (which were used to guide earlier treatment with external beam radiation therapy), two approaches are proposed to determine θ. If the patient has fiducial markers, then a point-based

rigid registration between fiducial points on the fresh and *in vivo* images is used to obtain θ. Alternatively, fresh images are digitally resampled at several different angles and visually compared to *in vivo* images to find the best match. To evaluate the accuracy of estimating θ, a metric denoted by Δ is developed. This metric measures the agreement between the relative position of the urethra with respect to the prostate boundary between *in vivo* MR and fresh *ex vivo* MR:

$$\Delta = \sum_{i=1}^{m} \left(\frac{d_a^{in}(i)}{d_p^{in}(i)} - \frac{d_a^{ex}(i)}{d_p^{ex}(i)} \right)^2$$

where $d_a^{in}(i)$ is the vertical distance of the urethra to the anterior part of the prostate boundary in the *in vivo* MR slice number i, and m is the number of corresponding slices on both *in vivo* MR and fresh that the urethra is visible. Superscript *ex* and subscript p represent the *ex vivo* fresh MR and vertical distance of the urethra to the posterior part of the prostate boundary, respectively. The vertical distances are determined by manual measurements. According to its definition, Δ is unitless. Ideally, Δ should be zero in case where the position of urethra in the *ex vivo* fresh MR exactly matches with that of the *in vivo* MR. Therefore, it is expected to have a smaller Δ for the resampled fresh MR with the estimated Δ. Table 1 shows that for all four patients Δ has been well reduced after resampling the fresh image set with the estimated θ. The angles are rounded up to multiples of 5° due to technical precision limit of the device used to cut the specimens. Further investigations on the proposed metric (Δ) and also to determine the accuracy of θ are ongoing.

Once estimated θ is verified by an expert radiation oncologist, the fixed specimen is sectioned at that angle with 3 mm slice thickness to replicate the thickness of the MR *in vivo* imaging. Digital photographs of these gross slices are then taken.

3D Reconstruction of Histology
Unlike the MR images which are inherently a 3D image, the whole-mount histology slices must be first reconstructed into a 3D volume to enable deformable registration to the corresponding images. To compensate for the deformations and misalignment between histology slices, each histology slice is first registered to its corresponding gross slice using a 2D deformable registration based on moving least squares (MLS).[14] The MLS algorithm is a landmark-based registration that warps the image using a locally rigid transformation based on the displacement of the control points. These control points are landmarks manually identified on the prostate boundary and urethra on the gross slice and corresponding histology slice. It should be noted

Table 1: Estimated sectioning angles denoted with θ (in degrees) and their errors based on the similarity of position of the urethra to the *in vivo* MR, represented by θ, before and after resampling fresh imageset with the estimated θ. Δ is unitless

Patient ID	θ (in degrees)	Δ Before	Δ After
A	20	1.19	0.54
B	5	0.62	0.48
C	20	1.04	0.33
D	25	7.80	0.15

Figure 2: Histology reconstruction. (a) 2D rigid registration between gross slices and their corresponding fixed images. (b) 2D deformable registration based on MLS between histology slides and gross slices

that the gross slices are not naturally aligned due to the manual setup of each slice to obtain digital photographs. Therefore, prior to registering histology to gross slices, a 2D rigid registration is performed between gross slices and the resliced fixed MR image set at the estimated θ. The rationale behind the use of the fixed image set is twofold: first, gross slices are acquired from the fixed tissue by 3 mm sectioning with the estimated θ and second, the magnitude of deformation to the tissue is minimum compared to other states (i.e., fresh and *in vivo*). The only source of deformation between the fixed MRI and gross slices is serial sectioning, which has been empirically observed to be small. Second, the fixed image set is already aligned since the images are obtained from the whole specimen. The urethra, the prostate boundary, and other anatomical features were used to guide the manual 2D rigid registration between gross slices and the resliced fixed image set with 3 mm slice thickness. The entire process is illustrated in Figure 2 part (a) shows the 2D rigid registration between gross slices and the resliced fixed image, while part (b) displays the 2D deformable registration based on MLS to obtain the warped histology slides. Finally, the prostate boundary is contoured on each warped histology slice using MIPAV (NIH, Bethesda, MD, USA). These contours are then converted into a 3D triangular mesh using an implementation of the marching cube algorithm. The 3D triangular mesh is then used in the biomechanical registration.

Deformable Registration Workflow

The proposed biomechanical model-based deformable registration workflow based on finite element modeling (FEM) consists of a three-step registration [Figure 1]. A 3D triangular surface mesh of each image set is reconstructed based on the delineated prostate boundary contours. At each registration step, a primary 3D volumetric FEM is registered to a secondary 3D surface mesh. A volumetric mesh is constructed using Hypermesh software (HyperWorks 10.0, Altair Engineering Inc., MI, USA) with tetrahedral elements based on the 3D triangular surface mesh. Appropriate material properties are then assigned to the 3D FEM of the primary based on the MRE results. Boundary conditions are obtained from projection of the primary surface nodes to the surface of
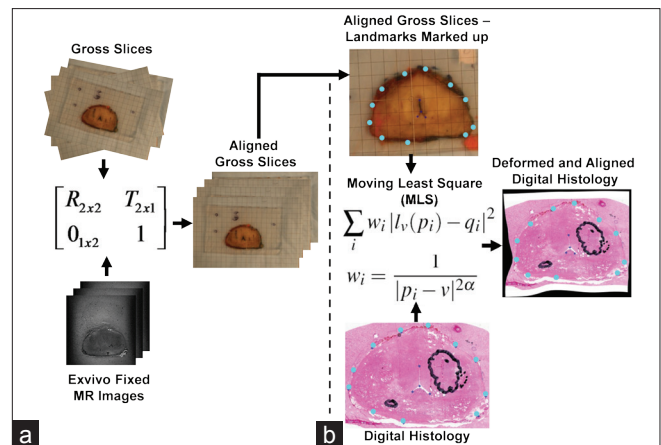
the 3D model of the secondary. Next, a commercial finite element analysis (FEA) package (Abaqus, v6.9, Abaqus Inc., Providence, RI, USA) finds the displacement of each node in the 3D tetrahedral mesh of the primary by solving the constitutive equations derived from the boundary conditions and the material models.

In the proposed three-step registration illustrated in Figure 1 different distortions and deformations are resolved by means of biomechanical modeling. First, geometric changes due to microtome sectioning and shrinkage are partially compensated by 2D deformable registration using the MLS technique. However to further increase the accuracy and to account for out-of-plane deformations, a uniform linear elastic 3D FEM of histology is built. This 3D model is then deformed to the fixed state using the biomechanical deformable registration as denoted by T_1^2. Second, changes due to fixative solution and dehydration during the fixation process are modeled in the next step of deformable registration represented as T_2^3. In this step, the result of T_1^2 is deformed to the fresh state. The last step, T_3^4, models the differences occurred between the *in vivo* and the fresh *ex vivo* MRI by deforming the result of T_2^3 to *in vivo*. These deformations are mainly due to the pressure caused by the endorectal coil at the time of *in vivo* scan and blood loss in the *ex vivo* imaging because of prostatectomy. Thus, the registration of histology to fixed (T_1^2) is based on a homogenous elastic material model, while the registrations of fixed to fresh (T_2^3) and the fresh to the *in vivo* (T_3^4) are performed using a heterogeneous specimen-specific material property model.

Development of the Material Model

A quasi-static MRE technique[13] is used to acquire 3D voxel-wise Young's modulus (E) maps of the prostate specimen with linear elasticity assumption in the fresh and the fixed states. Initial validation of this technique using canine prostate showed that the obtained E values

were accurately comparable with those measured by elastometer indentations.[13] Prior to correlating the E maps to the FEM, unrealistic values of Young's modulus due to MRI artifacts are detected by setting lower and upper thresholds, i.e., magnetic susceptibility artifacts due to air pockets between the gel could lead to errors in the calculated E maps.[13] The lower threshold for the fresh and the fixed MRE scans varied between 10e4 and 10e-2 KPa for different patients. The frequency of such values is less than 1% on average between patients. This value is chosen based on the fact that 1st percentile was decreased by more than 100% comparing with 0.9th percentile. Therefore, values less than this threshold can be considered as noise. The upper threshold is determined based on a comparison between 99.9th percentile and 99th percentile. If the difference between the two values is more than the 99th percentile value, then the values of 99.9th percentile is chosen as the upper threshold. Upper thresholds for the MRE scans varied between 500 KPa and 1500 KPa for different patients. Values higher than the upper threshold and values lower than the lower threshold are considered too high and too low, respectively. These noisy values are then replaced with the median of their surrounding normal values. Finally, a 3D Gaussian filter with the standard deviation of 4 is applied to the entire volume of the MRE data to further reduce the effect of noise and artifacts (see left part of the Figure 3). A method is proposed to find the element-voxel relation between 3D tetrahedral FEM of each state and its corresponding E maps. After matching the center of geometry of the 3D FEM and that of the prostate MRE data, the center of geometry of each tetrahedral element will fall in one of the voxels of the 3D E maps. Therefore, each element is assigned to its corresponding E values measured by the MRE technique as visualized in the right hand side of Figure 3.

Registration Evaluation

Target registration error (TRE) was used to quantitatively evaluate the deformable registration performance over rigid registration.[15] For T_i^j, TRE is defined as the Euclidean distance between the naturally occurring anatomical points identified on image set j and the transformed position of their corresponding points on image set i

$$TRE = \left\| T_i^j(P_i) - P_j \right\|,$$

where P_i and P_j are the corresponding points on imageset i and imageset j, respectively. In this work, rigid and deformable transformations obtained from the registrations are used to calculate TRE. It is important to note that none of the registration algorithms (deformable or rigid) rely on these naturally occurring anatomical points. Therefore, TRE presented in this work provides completely unbiased results. More particularly, T_i^j is not found based on the corresponding points (i.e., P_i and P_j).
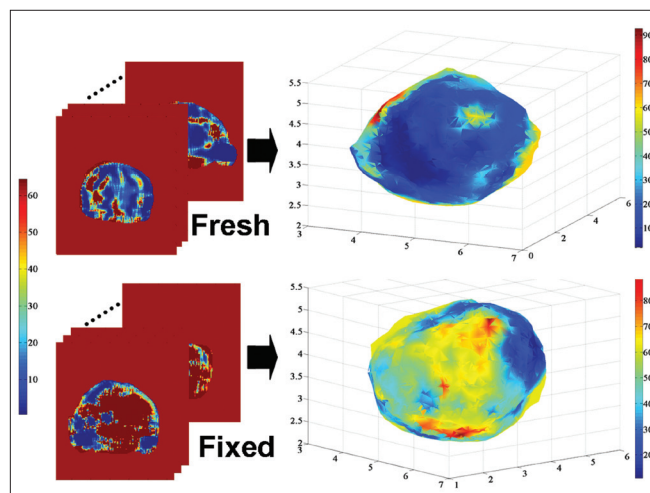
Figure 3: Material model construction based on MRE data. Each element of the model is assigned an E value from the MRE data. The top and the bottom left image sets are the MRE fresh and fixed scans, respectively. The top and the bottom right images display the reconstructed FEM after assigning the E values from MRE. The axes on the right side images represent the position in centimeter. Color maps show the E values in KPa. In the fresh-state E-maps variations in E were noted for diseased tissue and across normal anatomy. Fixation increases Young modulus nonuniformly and as an approximate function of distance from the tissue edge

In fact, the deformable transformation is found based on the constitutive equations derived from the boundary conditions and the material models.

Distances between surfaces of the histology and fixed 3D meshes were also used to compare rigid and deformable registration performance more clearly for histology to fixed registration step. More specifically, minimum distances of the nodes on the surface of the registered histology mesh to the surface of the fixed mesh (represented by triangular elements) were calculated.

RESULTS

The analysis has been completed on four patients. Table 2 represents mean, standard deviation, and the 90th percentile that shows the value that 90% of the TRE values fall below for each intermediate deformable and rigid registration step and also for the overall deformable and rigid registrations. For each step, different sets of points were chosen, although some of the points were used in multiple steps. This is due to the fact that these naturally occurring anatomical points cannot be found consistently on each image set because of differences in imaging modalities or the specimen condition. Therefore, the overall accuracy is not necessarily computable based on TRE of intermediate steps. The average number of points for all the steps and the patients was 30. From Table 2, it is noticeable that the proposed deformable registration has achieved better accuracy compared to rigid registration. However, the registration accuracy

Table 2: TRE (in mm) for all rigid and deformable registrations steps and the overall. The first column shows the patient ID. FEM denotes the proposed deformable registration using a MRE model. The last two columns of each step represent the value that 90% of TRE values fall below. The average number of naturally occurring anatomical points for all the patients is 30

Patient ID	Histology to fixed T_1^2				Fixed to fresh T_2^3			
	FEM	Rigid	FEM	Rigid	FEM	Rigid	FEM	Rigid
	Mean ± SD	Mean ± SD	90th %ile	90th %ile	Mean ± SD	Mean ± SD	90th %ile	90th %ile
A	2.5 ± 1.1	3.2 ± 1.6	4.5	5.5	2.4 ± 0.7	2.6 ± 0.9	3.4	3.7
B	3.3 ± 1.3	3.5 ± 1.6	5.0	5.5	2.1 ± 0.6	2.2 ± 0.8	2.9	3.4
C	2.6 ± 0.7	2.6 ± 1.1	3.6	3.8	2.3 ± 0.8	2.7 ± 0.8	3.7	4.2
D	3.4 ± 1.1	3.7 ± 1.4	4.6	5.9	1.8 ± 0.8	1.9 ± 0.6	2.7	2.7

Patient ID	Fresh to *in vivo* T_3^4				Histology to *in vivo* T_1^4			
	FEM	Rigid	FEM	Rigid	FEM overall	Rigid	FEM overall	Rigid
	Mean ± SD	Mean ± SD	90th %ile	90th %ile	Mean ± SD	Mean ± SD	90th %ile	90th %ile
A	2.2 ± 1.1	2.7 ± 1.4	4.1	4.8	2.1 ± 0.6	2.3 ± 0.7	2.9	3.4
B	2.3 ± 1.1	2.4 ± 1.3	4.0	4.5	2.2 ± 0.6	2.4 ± 0.9	3.0	3.3
C	3.8 ± 1.1	5.6 ± 0.8	5.4	6.6	2.9 ± 0.5	4.7 ± 0.5	3.3	5.5
D	2.6 ± 0.8	3.1 ± 1.3	3.6	4.8	2.5 ± 0.3	2.7 ± 1.1	2.8	4.4

obtained using rigid registration shows that the extent of deformations in the patients analyzed to date is small. Therefore, large differences between the performances of the proposed deformable registration and rigid registration are not expected. Although the proposed deformable registration average performance is modestly better than rigid, error improvements illustrated by a decrease of up to 1.3 mm in the 90th percentile between deformable and rigid registration could potentially have a clinical influence on the correlation of MRI and histology. It is also worth mentioning that because all the registration methods in this paper are performed in 3D, the error values are influenced by the voxel size of the images, which is 0.27 × 0.27 × 3 mm in the *in vivo* images.

It is important to note that in the proposed deformable registration workflow which consists of three steps, the goal is to incrementally refine the deformations by obtaining measured biomechanical properties based on two *ex vivo* MR scans: fresh MRE immediately after the surgery and fixed MRE after approximately 60 hours of fixation. Therefore, the possibility of error accumulation due to several registration steps must be considered with the trade-off of providing the biomechanical modeling deformable registration with more information about the mechanical properties of the specimen measured with MRE.

Table 2 also shows that in the histology to fixed registration step the performance of both rigid and deformable registrations is comparable. It should be noted that TRE is a local measure of accuracy and increasing the number of points where the TRE is calculated can help to

Table 3: Average, standard deviation, 90th percentile value of the distance between the histology and fixed surfaces (in mm) for step 1 (T_1^2) after rigid and deformable (denoted by FEM) registrations

Patient ID	FEM	Rigid	FEM	Rigid
	Mean ± SD	Mean ± SD	90th %ile	90th %ile
A	0.15 ± 0.21	1.61 ± 1.07	0.32	3.10
B	0.15 ± 0.21	1.23 ± 0.78	0.36	2.39
C	0.15 ± 0.24	1.76 ± 1.10	0.36	3.23
D	0.18 ± 0.26	3.4 ± 2.1	0.42	6.30

ensure that the TRE adequately represents the accuracy of local deformation occurring between the prostate images. Therefore, in addition to TRE to demonstrate the effectiveness of deformable registration over rigid registration, the distance between the 3D surfaces of the prostate between histology and fixed with rigid and deformable registration is also calculated. Table 3 shows that with rigid registration the 90th percentile of the distances reaches up to 6.3 mm (for patient D) whereas the 90th percentile value is limited to 0.42 mm (for patient D) with the proposed deformable registration algorithm. Such large surface distances obtained with rigid registration can cause significant issues when comparing histology and fixed images in cases where a small tumor is located close to the boundary of the prostate.

TRE distribution in three anatomical directions for the overall histology to *in vivo* registration resulted in 1.2 ± 0.4 mm (mean ± std) in left-right (LR), 0.9 ±

0.4 mm in anterior-posterior (AP), and 1.4 ± 0.5 mm in superior-inferior (SI) directions using the proposed deformable registration compared to 1.4 0.2 mm (LR), 1.6 ± 0.6 mm (AP), and 1.6 ± 1.4 mm (SI) obtained using rigid registration. Compared to published results by Zhan *et al*.[9] with average TRE of 0.82 mm between histology and *ex vivo* MR images, the TRE results of histology to fixed registration step (T_1^2) in this work are larger with the average of 2.9 mm. This difference can be explained by the fact that Zhan *et al*.[9] used 1.5 mm thick histology slices which was further reduced to 0.75 mm by interpolation. It is understandable to achieve submillimeter errors with the reduction of slice thickness from 3 mm to 0.75 mm. Additionally, visual comparison between the *ex vivo* MR images indicates that Zhan *et al*.[9] obtained images with more distinguishable features. One of the future goals of this work is to improve the *ex vivo* MR quality by optimizing the MRI acquisition parameters for prostate specimen. Ward *et al*.[10] achieved TRE of 0.85 mm with a 2D TPS registration between histology and *in vivo* MR based on leave-one-out cross-validation experiment using the fiducial points that guide the TPS registration. Since Ward *et al*.[10] obtained histology slices with approximately perpendicular to SI direction cuts, the overall TRE distribution of 1.2 mm in LR and 0.9 mm in AP achieved in this work is comparable with their reported TRE of 0.85.

Figure 4 illustrates a visualization of a corresponding slice between all the image sets after each registration step in the proposed workflow. Figure 4a-d represent the *in vivo*, fresh, fixed, and histology of a corresponding slice. Figure 4e displays the checkerboard visualization of the *in vivo* and deformed histology. The checkerboard visualization of the deformed fresh and *in vivo* is shown in Figure 4f. The alignment between deformed fixed and fresh images is visualized in Figure 4g. Finally, Figure 4h represents a satisfying alignment between deformed histology and the fixed *ex vivo* MR. It should be noted that the small black region under the urethra on the *in vivo*, fresh, and fixed image sets shows one of the gold seeds, and it corresponds to the white region under the urethra on the histology since the actual seed was removed during the sectioning process. Most of the corresponding slices between each image sets have achieved a similar qualitative performance after the proposed deformable registration which indicates an overall good quality of registration.

CONCLUSION

Histology to MR correlation is challenging due to various deformations in the tissue. In this paper, a proof of concept deformable registration workflow is proposed which is primarily based on biomechanical modeling. The registration workflow is shown to be a
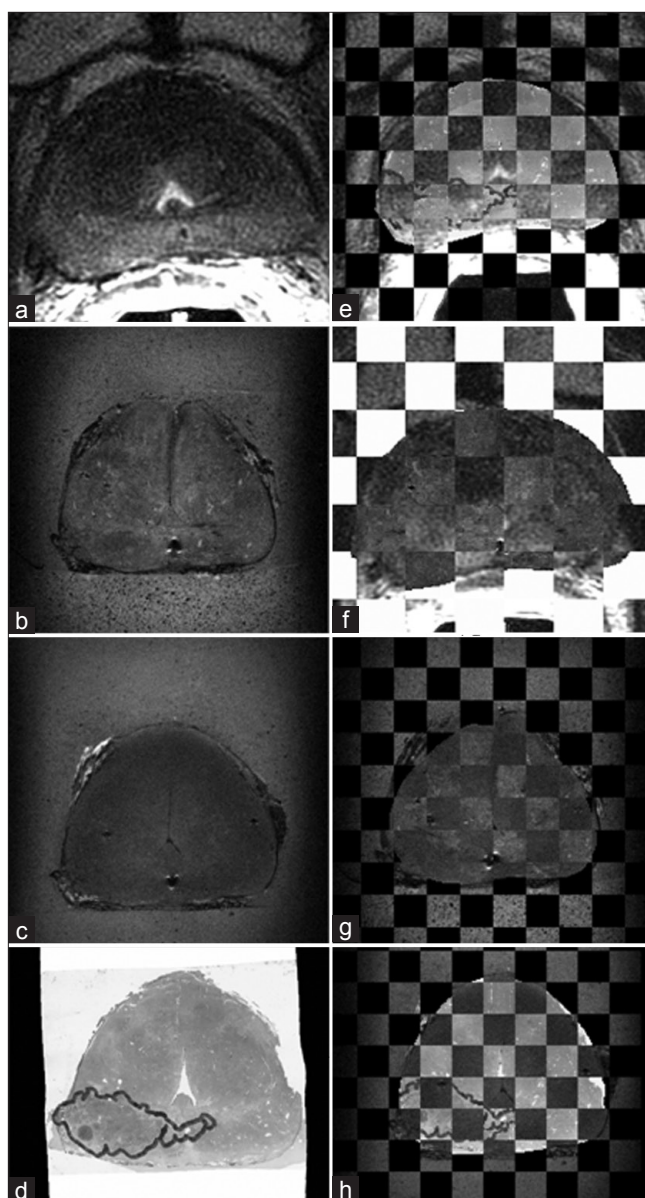
Figure 4: Checkerboard visualization for different registration steps in the proposed workflow. Figures (a)-(d) show the corresponding slice on *in vivo*, fresh, fixed, and the histology, respectively, (e) is the checkerboard display of the deformed histology overlaid on the *in vivo*. (f) shows the deformed fresh image overlaid on the *in vivo*, (g) represents the fresh image overlaid on the deformed fixed, (h) is the overlay of the deformed histology on the fixed image

promising technique for correlating histological slides of the prostate specimen to *in vivo* MRI. The addition of two intermediate steps of the prostate specimen (fresh and fixed) including the specimen-specific linear elastic heterogeneous material models built from MRE data provides useful information about the extent of deformations during the fixation process. The validation of the proposed technique using four patients resulted in the average TRE of 2.3 mm, which is in the order of the slice thickness, 3 mm. The current overall level of accuracy can be improved by using higher resolution (i.e., smaller slice thickness) *in vivo* images. Highly accurate

registration of histology to high resolution *ex vivo* images before and after fixation provides unique information for future clinical investigations.

ACKNOWLEDGMENTS

REFERENCES

1. Jaffray DA, Siewerdsen JH, Wong JW, Martinez AA. Flat-panel cone-beam computed to-mography for image-guided radiation therapy. Int J Radiat Oncol Biol Phys 2002;53:1337-49.
2. Jeanneret-Sozzi W, Moeckli R, Valley JF, Zouhair A, Ozsahin EM, Mirimanoff RO. The reasons for discrepancies in target volume delineation. Strahlenther Onkol 2006;182:450-7.
3. Teh BS, Bastasch MD, Wheeler TM, Mai W, Frolov A, Uhl BM, *et al*. IMRT for prostate cancer: defin-ing target volume based on correlated pathologic volume of disease. Int J Radiat Oncol Biol Phys 2003;56:184-91.
4. Rueckert D, Sonoda LI, Hayes C, Hill DL, Leach MO, Hawkes DJ. Nonrigid registration using free-form deformations: Application to breast MR images. IEEE Trans Med Imaging 2002;18:712-21.
5. Dauguet J, Delzescaux T, Condé F, Mangin JF, Ayache N, Hantraye P, *et al*. Three-dimensional reconstruction of stained histological slices and 3D non-linear registration with *in vivo* MRI for whole baboon brain. J Neurosci Methods 2007;164;191-204.
6. Alic L, Haeck JC, Klein S, Bol K, Van Tiel ST, Wielopolski PA, *et al*. Multi-modal image registration: Matching MRI with histology. in Proceedings of SPIE 2010;7626:762603-1-9.
7. Chappelow J, Bloch BN, Rofsky N, Genega E, Lenkinski R, DeWolf W, *et al*. Elastic registration of multimodal prostate MRI and histology via multiattribute combined mutual information. Med Phys 2011;38:2005-18.
8. Mazaheri Y, Bokacheva L, Kroon DJ, Akin O, Hricak H, Chamudot D, *et al*. Semi-automatic deformable registration of prostate MR images to pathological slices. J Magn Reson Imaging 2010;32:1149-57.
9. Zhan Y, Ou Y, Feldman M, Tomaszeweski J, Davatzikos C, Shen D. Registering Histologic and MR Images of Prostate for Image-based Cancer Detection. Acad Radiol 2007;14:1367-81.
10. Ward A, Crukley C, McKenzie C, Montreuil J, Gibson E, Gomez J, *et al*. Registration of *in vivo* prostate magnetic resonance images to digital histopathology images. Prostate Cancer Imaging. Computer-Aided Diagnosis, Prognosis, and Intervention, Lect Notes Comput Sci 2010;6367:66-76.
11. Ceritoglu C, Wang L, Selemon LD, Csernansky JG, Miller MI, Ratnanather JT. Large deformation diffeomorphic metric mapping registration of reconstructed 3D histological section images and *in vivo* MR images. Front Hum Neurosci 2010;4:43.
12. McNiven A, Moseley J, Langer DL, Haider MA, Brock KK. Preliminary Feasibility Study: Modeling 3D deformations of the prostate from whole-mount histology to in vivo MRI. Med Phys 2009;36:2567.
13. McGrath DM, Foltz WD, Brock KK. Measuring the Effect of Formalin Fixation on *Ex vivo* Tissue Material Properties using High Resolution 3D Quasi-Static MR Elastography at 7 Tesla for Improved Biomechanical Registration of Histopathology, and Correlation with the Effect of Fixation on T1, T2 and ADC. Proc Intl Soc Mag Res Med 2010;18:2504.
14. Schaefer S, McPhail T, Warren J. Image deformation using moving least squares. ACM Transactions on Graphics (TOG) 2006;3:533-40.
15. Besl PJ, McKay ND. A method for registration of 3-D shapes. IEEE Trans Pattern Anal Mach Intell 1992;239-56.